

UAV Relay-assisted NOMA MEC in IoT networks: Offloading Performance and Optimization

Anh-Nhat Nguyen, Tien-Dung Do, Gia-Huy Nguyen, and Hien-Hieu Le

Department of Computing Fundamentals, FPT University, Hanoi, Vietnam

nhatna3@fpt.edu.vn

{dungdthe170502, huyngh180064, hieulhhe181040}@fpt.edu.vn

Abstract. This paper investigated how unmanned aerial vehicles (UAVs) can enhance nonorthogonal multiple access (NOMA) mobile-edge computing (MEC) in the Internet of Things (IoT) by acting as relay stations for ground base stations (BSs). We derived closed-form formulations for successful computation probability (SCP) in accordance with Nakagami- m fading modelled for assessing system effectiveness. Furthermore, we provided a SCP maximization problem that improved UAV deployment location using the particle swarm optimization (PSO) method. Finally, numerical results demonstrated that parameters such as UAV's transmit signal-to-noise ratio (SNR), edge devices (EDs)' number, antennas of BS, and UAV deployment location significantly impacted system offload performance, which is confirmed by Monte Carlo simulations.

Keywords: mobile-edge computing, unmanned aerial vehicle, nonorthogonal multiple access

1 Introduction

The demand for mobile data traffic in Internet of Things (IoT) has seen a substantial increase in recent years. However, mobile devices, which have limited energy and computational capabilities, encounter difficulties in meeting the growing demand for applications that require continuous and intensive processing. These applications encompass areas like virtual and augmented reality, remote operations, and autonomous driving [1].

To solve the challenges, researchers suggest mobile-edge computing (MEC) and nonorthogonal multiple access (NOMA) for IoT networks [2]. MEC enables mobile devices to compute using nearby computational resources. NOMA, on the other hand, allows multiple mobile devices to share a time/frequency resource block in the power domain. NOMA transmission and reception employ superposition coding and successive interference cancellation (SIC) [3]. MEC modes that are commonly used are partial and binary computation offloading [4]. Offloading efficiency has recently been increased by combining NOMA-based MEC systems [5, 6]. In [5] investigates two NOMA offloading scenarios, whereas in [6]

investigates a NOMA MEC system with two clusters of edge devices (EDs) linked by a multi-antenna access point.

Nonetheless, the effectiveness of MEC relies heavily on the transfer of data and computational processes between devices and servers. Signal reception efficiency can be compromised due to the unpredictable positioning of EDs. Most EDs have limited power characteristics, which consequently limit their transmission range. Employing wireless communication with UAVs presents a potential technological solution to address these aforementioned limitations [7]. The key feature of UAV communication lies in the existence of Line-of-Sight (LoS) probabilities of UAV-EDs connections. These links offer several advantages, such as reduced small-scale fading, potential enhancements in network performance, and the UAV's ability to provide signal coverage, a feature underscored in prior research [8]. Furthermore, UAVs have the capability to approach EDs at close range, ensuring the establishment of reliable communication connections. Therefore, UAVs can function as a reliable and versatile means of transporting an edge server [9] or as a relay for EDs and BSs [10].

This study investigates at offloading efficiency in IoT networks using UAV relay-supported NOMA-MEC over Nakagami- m fading channels. We take into account the presence of LoS and non-LoS (NLoS) scenarios in wireless communication between UAV and ground devices. Finally, we offer an optimization problem to improve offloading performance. The main contributions of our paper are as follows:

- We consider an ED and antenna selection scheme for UAV relay-supported NOMA-MEC in IoT networks over Nakagami- m fading. Consequently, a communication protocol is presented for an effective dispatching procedure.
- We obtain closed-form SCP expressions for the entire system. We also address the UAV deployment location optimization challenge to maximize SCP by using PSO algorithm.
- We use numerical results such as transmit power, EDs' number, antennas' number, and UAV deployment location to confirm the efficacy of our system.

The rest of this paper is structured as follows. Section 2 introduces the system model and communication protocol. Section 3 analyzes SCP and optimization problem. In Section 4, numerical results are presented and discussed. Finally, conclusions are presented in Section 5.

2 System Model and Communication Protocol

2.1 System model

As shown in Fig. 1, we consider a amplify-and-forward (AF) UAV relay comprising downlink NOMA-MEC in IoT network [3], denoted by U_R , which helps an ED cluster, denoted by $I_i, 1 \leq i \leq N$, in offloading tasks to the far BS-MEC1 has M antennas, denoted by $B_{1,j}, 1 \leq j \leq M$, and the near BS-MEC2 has K antennas, denoted by $B_{2,k}, 1 \leq k \leq K$ via U_R . All system components are

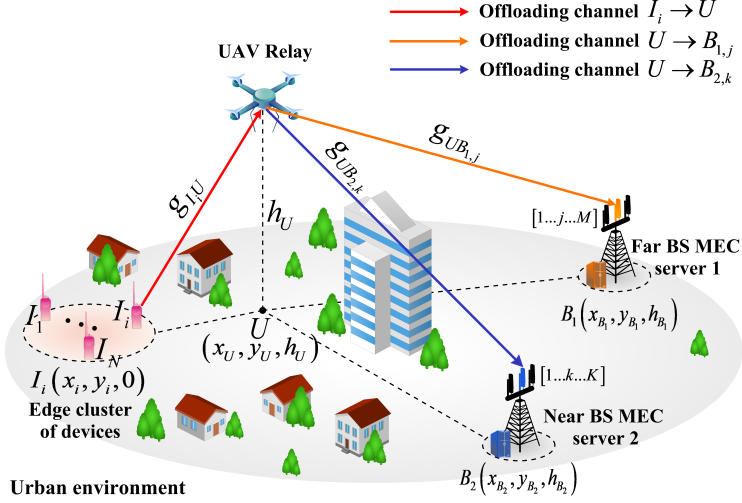


Fig. 1: System model for a UAV relay-assisted NOMA-MEC in the IoT network.

in the half-duplex mode, and the appearance of impediments in urban environments disrupts the feasibility of BSs-EDs direct links [10]. We utilize a 3D Cartesian coordinate system, used $U(x_U, y_U, h_U)$, where $h_U > 0$; $B_1(x_{B_1}, y_{B_1}, h_{B_1})$; $B_2(x_{B_2}, y_{B_2}, h_{B_2})$; and $I_i(x_i, y_i, 0)$. Assuming the fading channels of UAV and EDs are guided by a LoS and NLoS probabilistic model. Hence, the mean path loss between U and ground devices is estimated as [11]:

$$\mathcal{L}_{ab}(d_{ab}, \varphi_{ab}) = \left[\mathcal{P}_{LoS} + \frac{\mathcal{P}_{LoS} - \mathcal{P}_{NLoS}}{1 + \mathcal{B}e^{(-\frac{180}{\pi}\mathcal{A}\varphi_{ab} + \mathcal{A}\mathcal{B})}} \right] d_{ab}^{\sigma}, \quad (1)$$

where $ab \in (I_i U_R, U_R B_{1,j}, U_R B_{2,k})$, the elevation angle $\varphi_{ab} = \arcsin\left(\frac{h_U}{d_{ab}}\right)$ and the ab distance is $d_{ab} = \sqrt{(x_b - x_a)^2 + (y_b - y_a)^2 + h_U^2}$; σ is the path-loss exponent; \mathcal{A} and \mathcal{B} are constant values influenced by the environment conditions; and $\mathcal{P}_{\kappa} = \mathcal{O}_{\kappa}(c/4\pi f_c)^{-1}$, where $\kappa \in \{LoS, NLoS\}$, \mathcal{O}_{κ} and f_c are the excessive path-losses of LoS and NLoS communications and the carrier frequency, and c is the speed of light.

The EDs are assumed to be executing the same workloads comprising tasks of length L (bits) and distinct tasks are split into discrete groups [6]. Two BSs are supposed to be in different areas and both have MEC servers. The B_1 is far from U_R , while B_2 is close to U_R . U_R is aided in forwarding tasks from I_i and separating them into two sub-tasks; The first sub-task is denoted as $C_1^{off} = \beta L$ (bits) transferred to B_1 , while the second sub-task is denoted by $C_2^{off} = (1-\beta)L$ (bits) transferred to B_2 , where β ($0 \leq \beta \leq 1$) is the offloading ratio.

2.2 Channel model

Let g_{ab} be the channel coefficients from $a \rightarrow b$. We assume that all channels follow Nakagami- m fading, where m is fading parameter and g_{ab} is random variable (RV) distributed following the Nakagami- m model [2]. We propose a scheme for selecting the best ED to offload tasks to UAV and the best antenna to receive offloaded tasks from UAV. Specifically, the I_i simultaneously transmits pilot signals to U_R [13]. U_R estimates the SNRs of all transmission channels and selects the best ED, designated I_* as signals with the greatest received SNR at U_R . Therefore, the chosen ED's channel power gain in the cluster is as follows:

$$|g_{I_* U_R}|^2 = \arg \max_{1 \leq i \leq N} (|g_{I_i U_R}|^2). \quad (2)$$

Similar to selecting ED, U_R transmits pilot signals to M antennas at B_1 and K antennas at B_2 , simultaneously. Once the SNRs of all U_R to $B_{1,j}$ and $B_{2,k}$ channels have been estimated, the best antennas are determined, designated as $B_{1,*}$ and $B_{2,*}$. Therefore, the channel power gains of the best antennas in the B_1 and B_2 are:

$$|g_{U_R B_{1,*}}|^2 = \arg \max_{1 \leq j \leq M} (|g_{U_R B_{1,j}}|^2), \quad (3)$$

$$|g_{U_R B_{2,*}}|^2 = \arg \max_{1 \leq k \leq K} (|g_{U_R B_{2,k}}|^2). \quad (4)$$

In this work, the fading parameter m between links was constrained to be integer and the value was assumed to be the same for all links. Hence, the probability density function (PDF) and cumulative distribution function (CDF) of the channel gain $|g_\psi|^2$, $\psi \in (I_* U_R, U_R B_{1,*}, U_R B_{2,*})$ are given as [14]:

$$f_{|g_\psi|^2}(y) = \frac{\Xi y^{m-1}}{(m-1)!} \left(\frac{m}{\Omega_\psi} \right)^m \sum_{\tau=0}^{\Xi-1} \bigcup_{\tau} (-1)^\tau \Theta_{1,\tau} \Theta_{2,\tau} y^{\bar{\tau}} e^{-\frac{my(\tau+1)}{\Omega_\psi}}, \quad (5)$$

$$F_{|g_\psi|^2}(y) = \sum_{\tau=0}^{\Xi} \bigcup_{\tau} (-1)^\tau \Theta_{1,\tau} \Theta_{2,\tau} y^{\bar{\tau}} e^{-\frac{tm_y}{\Omega_\psi}}, \quad (6)$$

where $\Xi \in \{N, M, K\}$, $\Omega_\psi = \mathbf{E} \left\{ |g_\psi|^2 \right\}$, and \bigcup_{τ} , $\Theta_{1,\tau}$, $\Theta_{2,\tau}$ and $\bar{\tau}$ are defined as follows:

$$\bigcup_{\tau} = \sum_{\tau_1=0}^{\tau} \sum_{\tau_2=0}^{\tau-\tau_1} \dots \sum_{\tau_{(m-1)}=0}^{\tau-\tau_1-\dots-\tau_{(m-2)}}, \quad (7)$$

$$\Theta_{1,\tau} = \binom{\Xi}{\tau} \binom{\tau}{\tau_1} \binom{\tau-\tau_1}{\tau_2} \dots \binom{\tau-\tau_1-\dots-\tau_{(m-2)}}{\tau_{(m-1)}}, \quad (8)$$

$$\Theta_{2,\tau} = \prod_{s=0}^{m-2} \left[\frac{1}{s!} \left(\frac{m}{\Omega_\psi} \right)^s \right]^{\tau_{(s+1)}} \left[\frac{1}{(m-1)!} \left(\frac{m}{\Omega_\psi} \right)^{m-1} \right]^{\tau-\tau_1-\dots-\tau_{(m-1)}}, \quad (9)$$

$$\bar{\tau} = (m-1)(\tau - \tau_1) - (m-2)\tau_2 - (m-3)\tau_3 \dots - \tau_{(m-1)}. \quad (10)$$

2.3 Communication protocol

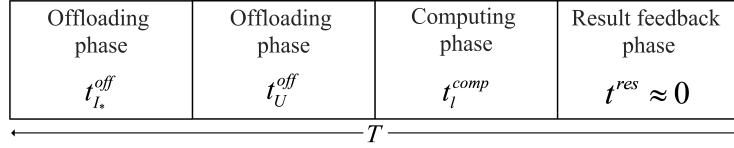


Fig. 2: Time flowchart of the considered UAV relay NOMA-MEC network.

This subsection describes the proposed system communication protocol in Fig 2. The following is the description of each phase.

- In the first phase ($t_{I_*}^{off}$): I_* offloads L bits to U_R . The signal retrieved at U is as follows:

$$y_{U_R} = \sqrt{\frac{P_{I_*}}{L_{I_* U_R}}} \left(\sqrt{\rho}x_1 + \sqrt{(1-\rho)}x_2 \right) g_{I_* U_R} + n_U, \quad (11)$$

where x_1 and x_2 are the offloaded signals to B_1 and B_2 , respectively; P_{I_*} is the transmit power of best ED; ρ is the power allocation coefficient, $0.5 < \rho \leq 1$; $n_U \sim \mathcal{CN}(0, N_0)$ is additive white Gaussian noise (AWGN).

- In the second phase, which has a duration of $t_{U_R}^{off}$, U_R offloads the received signal from I_* to $B_{l,*}, l \in (1, 2)$ by using downlink NOMA technique [11], the signal received at B_l is given by

$$y_{B_{l,*}} = \frac{G}{\sqrt{L_{U_R B_{l,*}}}} y_U g_{U_R B_{l,*}} + n_{B_l}, \quad (12)$$

where P_U is the transmit power of U_R , G is the amplifying factor of the AF transition scheme, denoted by $G = \sqrt{\frac{P_U L_{I_* U_R}}{P_{I_*} |g_{I_* U_R}|^2 + L_{I_* U_R} N_0}}$, and $n_{B_l} \sim \mathcal{CN}(0, N_l)$ is AWGN. Therefore, the received signal-to-interference-plus-noise ratios (SINRs) end-to-end at B_1 and B_2 for detecting x_1 and x_2 , respectively, are expressed as follows:

$$\gamma_1^{e2e} = \frac{\rho \gamma_0 \gamma_1 XY}{\gamma_1 [(1-\rho) \gamma_0 X + L_{I_* U_R}] Y + \gamma_0 L_{U_R B_{1,*}} X + L_{I_* U_R} L_{U_R B_{1,*}}}, \quad (13)$$

$$\gamma_2^{e2e} = \frac{(1-\rho) \gamma_0 \gamma_2 XZ}{\gamma_2 L_{I_* U_R} Z + \gamma_0 L_{U_R B_{2,*}} X + L_{I_* U_R} L_{U_R B_{2,*}}}, \quad (14)$$

where $X = |g_{I_* U_R}|^2$, $Y = |g_{U_R B_{1,*}}|^2$, $Z = |g_{U_R B_{2,*}}|^2$, $\gamma_0 = \frac{P_{I_*}}{N_0}$, $\gamma_1 = \frac{P_U}{N_1}$, and $\gamma_2 = \frac{P_U}{N_2}$. The instantaneous channel capacity of the $I_* \rightarrow B_{l,*}$ link is formulated as follows:

$$C_l^{x_l} = W \log_2 (1 + \gamma_{B_l}^{e2e}), \quad (15)$$

where W is the bandwidth. Hence, the time offloading from I_* to $B_{l,*}$ is given by

$$t_l^{off} = \frac{C_l^{off}}{C_l^{xi}}. \quad (16)$$

- In the third phase, t_l^{comp} : U engages in computational processing for the offloaded tasks. The duration required for the completion of computing these task bits at U is as follows:

$$t_l^{comp} = \frac{\varsigma C_l^{off}}{f_l^{MEC}}, \quad (17)$$

where ς is the number of CPU cycles required to run the calculation for a input bit and f_l^{MEC} is the MEC's operating frequency at B_l .

- In the fourth phase, t^{res} : B_l returns the computed results to I_* via U_R . The delay-time of sending back results from B_l to I_* are overlooked because the processed data are significantly smaller in package-size compared to the offloaded data [6].

3 Performance Analysis

3.1 Successful computation probability (SCP)

In this subsection, for the evaluations of UAV relay assisted downlink NOMA-MEC, we obtain closed-form expressions for the SCP designated as the likelihood for all offloaded tasks to be accomplished within a given time T . Therefore, the SCP can be formulated as follows [6, 13]:

$$S_l = \Pr \left\{ t_l^{off} \leq T_l^{th} \right\}, \quad (18)$$

where $T_l^{th} = T - t_l^{comp}$.

Lemma 1. *The closed-form formula for the SCP of the far BS-MEC for UAV relay-assisted NOMA-MEC under quasi-static Nakagami- m fading is as follows:*

$$\begin{aligned} S_1 = & 2\theta_1 \sum_{j=1}^M \sum_{j_1=0}^j \sum_{N-1}^{N-1} \sum_{i=0}^i \sum_{i_1=0}^{m+\bar{i}-1} \sum_{t_1=0}^{\bar{j}} \theta_2 \theta_3 \theta_4 (\varphi_1)^{m+\bar{i}-1-t_1} (\varphi_2)^{\bar{j}} \\ & \times (\varphi_4)^{\bar{j}-t_2} e^{-\frac{mj\varphi_2}{\Omega_1} - \frac{m(i+1)\varphi_1}{\Omega_I}} \left(\frac{j(\varphi_2\varphi_1 + \varphi_3)\Omega_I}{(i+1)\Omega_1} \right)^{\frac{t_1+t_2-\bar{j}+1}{2}} \\ & \times \mathcal{K}_{t_1+t_2-\bar{j}+1} \left(2m \sqrt{\frac{j(i+1)(\varphi_2\varphi_1 + \varphi_3)}{\Omega_1\Omega_I}} \right), \end{aligned} \quad (19)$$

where $\theta_1 = -\frac{NM!(N-1)!}{(m-1)!} \left(\frac{m}{\Omega_I}\right)^m$, $\theta_2 = \frac{(-1)^j}{(M-j)!j_1!(j-j_1)!} \frac{(-1)^i}{(N-1-i)!i_1!(i-i_1)!}$, $\theta_3 = \frac{(m+\bar{i}-1)!}{t_1!(m+\bar{i}-1-t_1)!} \frac{\bar{j}!}{t_2!(\bar{j}-t_2)!}$, $\theta_4 = \left[\frac{1}{(m-1)!} \left(\frac{m}{\Omega_I}\right)^{m-1}\right]^{j-j_1} \left[\frac{1}{(m-1)!} \left(\frac{m}{\Omega_I}\right)^{m-1}\right]^{i-i_1}$, $\varphi_1 = \frac{\phi_1 L_{I*U_R}}{\gamma_0 [\rho - (1-\rho)\phi_1]}$, $\varphi_2 = \frac{\phi_1 L_{U_RB_{1,*}}}{\gamma_1 [\rho - (1-\rho)\phi_1]}$, $\varphi_3 = \frac{\phi_1 L_{I*U_R} L_{U_RB_{1,*}}}{\gamma_0 \gamma_1 [\rho - (1-\rho)\phi_1]}$, $\varphi_4 = \frac{\varphi_2 \varphi_1 + \varphi_3}{\varphi_2}$, $\phi_1 = 2^{\frac{C_1^{off}}{WT_1^{th}}} - 1$ and $\mathcal{K}_v(\cdot)$ is Bessel function [15].

Proof. See Appendix A.

Lemma 2. The closed-form formula for the SCP of the near BS-MEC for UAV relay-assisted NOMA-MEC under quasi-static Nakagami-m fading is as follows:

$$\begin{aligned} S_2 = 2\lambda_1 \sum_{j=1}^K \sum_{j_1=0}^j \sum_{i=0}^{N-1} \sum_{i_1=0}^i \sum_{t_1=0}^{m+\bar{i}-1} \sum_{t_2=0}^{\bar{j}} \lambda_2 \lambda_3 \lambda_4 (\varphi_5)^{m+\bar{i}-1-t_1} (\varphi_6)^{\bar{j}} \\ \times (\varphi_8)^{\bar{j}-t_2} e^{-\frac{mj\varphi_6}{\Omega_2} - \frac{m(i+1)\varphi_5}{\Omega_I}} \left(\frac{j(\varphi_5\varphi_6 + \varphi_7)\Omega_I}{(i+1)\Omega_2} \right)^{\frac{t_1+t_2-\bar{j}+1}{2}} \\ \times \mathcal{K}_{t_1+t_2-\bar{j}+1} \left(2m \sqrt{\frac{j(i+1)(\varphi_5\varphi_6 + \varphi_7)}{\Omega_2\Omega_I}} \right), \quad (20) \end{aligned}$$

where $\lambda_1 = -\frac{NK!(N-1)!}{(m-1)!} \left(\frac{m}{\Omega_I}\right)^m$; $\lambda_2 = \frac{(-1)^j}{(K-j)!j_1!(j-j_1)!} \frac{(-1)^i}{(N-1-i)!i_1!(i-i_1)!}$, $\lambda_4 = \left[\frac{1}{(m-1)!} \left(\frac{m}{\Omega_I}\right)^{m-1}\right]^{j-j_1} \left[\frac{1}{(m-1)!} \left(\frac{m}{\Omega_I}\right)^{m-1}\right]^{i-i_1}$, $\varphi_5 = \frac{\phi_2 L_{I*U_R}}{(1-\rho)\gamma_0}$, $\varphi_6 = \frac{\phi_2 L_{U_RB_{2,*}}}{(1-\rho)\gamma_2}$, $\varphi_7 = \frac{\phi_2 L_{I*U_R} L_{U_RB_{2,*}}}{(1-\rho)\gamma_0\gamma_2}$, $\varphi_8 = \frac{\varphi_6\varphi_5 + \varphi_7}{\varphi_6}$, and $\phi_2 = 2^{\frac{C_2^{off}}{WT_2^{th}}} - 1$.

Proof. The proof is similar to that of Lemma 1.

3.2 Optimization

To enhance offloading performance, we focus on enhancing the B_l successful computation performance by establishing the optimal UAV deployment location, designated as (x_U^*, y_U^*, h_U^*) . In order to accomplish this, we formulate the SCP maximization problem and solve it using a PSO-based algorithm.

SCP maximization problem:

$$(P1): \underset{x_U, y_U, h_U}{\text{maximize}} \quad S_l \quad (21a)$$

$$\text{subject to} \quad x_U^{\min} \leq x_U \leq x_U^{\max}, \quad (21a)$$

$$y_U^{\min} \leq y_U \leq y_U^{\max}, \quad (21b)$$

$$0 \leq h_U \leq h_U^{\max}, \quad (21c)$$

Algorithm 1 SCPMax-PSO

Require: $\mathcal{N}, \mathcal{I}, S_l, \varpi, \chi, \epsilon_1, \epsilon_2$, and constraint conditions
Ensure: x_U^*, y_U^*, h_U^*

```

1: function SCP_MAX
2:   Set parameters of PSO:  $\mathcal{N}; \mathcal{I}; \varpi; \chi; \epsilon_1; \epsilon_2; \mathcal{G}_b = \infty;$ 
3:   for  $i = 1 : \mathcal{N}$  do                                 $\triangleright$  Initialize population members
4:     Generate random solution:  $\mathcal{X}_i(x_U, y_U, h_U); \mathcal{V}_i = 0;$ 
5:     Evaluation of particle  $i$ :  $\mathcal{C}_i = 1 - S_l(\mathcal{X}_i);$ 
6:     Update the personal best:  $\mathcal{X}_i^* = \mathcal{X}_i; \mathcal{C}_i^* = \mathcal{C}_i;$ 
7:     if  $\mathcal{C}_i^* < \mathcal{G}_b$  then
8:        $\mathcal{G}_b = \mathcal{C}_i^*;$ 
9:     end if
10:    end for
11:    for  $j = 1 : \mathcal{I}$  do                       $\triangleright$  Main loop of SCP-PSO algorithm
12:      for  $i = 1 : \mathcal{N}$  do
13:        Update velocity:  $\mathcal{V}_i = \chi \mathcal{V}_{i-1} + \epsilon_1 r_1 (\mathcal{X}_{i-1}^* - \mathcal{X}_{i-1})$ 
            $+ \epsilon_2 r_2 (\mathcal{X}_{\mathcal{G}_b, i-1} - \mathcal{X}_{i-1});$ 
14:        Update position:  $\mathcal{X}_i = \mathcal{X}_{i-1} + \mathcal{V}_i;$ 
15:        Evaluation of particle  $i$ :  $\mathcal{C}_i = 1 - S_l(\mathcal{X}_i);$ 
16:        if  $\mathcal{C}_i < \mathcal{C}_i^*$  then
17:           $\mathcal{X}_i^* = \mathcal{X}_i; \mathcal{C}_i^* = \mathcal{C}_i$ 
18:          if  $\mathcal{C}_i^* < \mathcal{G}_b$  then
19:             $\mathcal{G}_b = \mathcal{C}_i^*;$ 
20:          end if
21:        end if
22:      end for
23:      Store the best cost value:  $\mathcal{B}(j) = \mathcal{G}_b$ 
24:    end for
25:    return  $x_U^*, y_U^*, h_U^*;$ 
26: end function

```

where constraints (21a) and (21b) represent conditions on the UAV's projected location on the ground, constraint (21c) imposes conditions on the altitude of the UAV. We suggest the PSO algorithm [13], a population-based, stochastic method based on SI that can handle hard optimization problems, to solve the problem (29) with multiple constraints. The overall SCP maximization based on PSO algorithm (SCPMax-PSO) is shown in **Algorithm 1**. This algorithm is used for our suggested system model. At the start of the process, particles $i = [1, \mathcal{N}]$ are set up at random. For each particle i , the current position is $\mathcal{X}_i = (x_U, y_U, h_U)$, the current speed is \mathcal{V}_i , the personal best position is \mathcal{X}_i^* , which is where the particle had its greatest value for the SCP objective function, and the global best position is \mathcal{G}_b , which is the best position out of all the personal best positions. The SCPMax-PSO algorithm iterates \mathcal{I} times until the particle with the best \mathcal{X}_i^* and \mathcal{G}_b is discovered. After each cycle, the position \mathcal{X}_i , speed \mathcal{V}_i , and best values \mathcal{X}_i^* and \mathcal{G}_b of each particle are changed.

4 Numerical result

In this section, we provide numerical results for validating the SCP analytical expression obtained in Section 3 for the UAV-assisted NOMA-MEC in IoT network. Specifically, we consider the following parameters for all simulations [2,13] such as $P_U = [0, 20]$ (dB), $P_I = [0, 3]$ (dB), $L = 10^4$ (bits), $T = 1$ (s), $\rho = 0.75$, $\beta = 0.6$, $\mathcal{A} = 0.1581$, $\mathcal{B} = 9.6177$, $\mathcal{O}_{LoS} = 1$, $\mathcal{O}_{NLoS} = 20$, $c = 3.10^8$ (m/s), $W = 10^5$ (Hz), $f_c = 10^4$, $f_U^{MEC} = 10^8$, $\varsigma = 10^2$, $\mathcal{I} = 10^2$, and $\mathcal{N} = 10^2$.

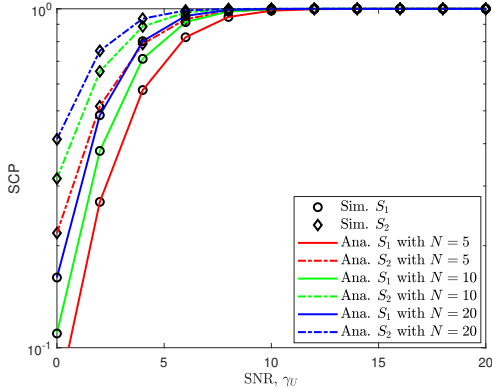


Fig. 3: Impact of average transmit SNR, (γ_U) on SCPs of the BS-MEC1 and BS-MEC2 with various N , $\gamma_0 = 1$, $(x_I, y_I) = (-100, -100)$, $(x_{B_1}, y_{B_1}, h_{B_1}) = (0, 200, 5)$, $(x_{B_2}, y_{B_2}, h_{B_2}) = (0, 150, 5)$, and $(x_U, y_U, h_U) = (0, 0, 150)$.

Illustrations of the effect of average transmit SNR (γ_U) on SCPs for the distinct EDs' number as shown in Fig. 3. The first thing we notice is that the analysis and simulation are perfectly consistent, indicating the validity of our suggested model. The second observation is that when we increase the EDs number, the system offload performance is enhanced. This can be described as the UAV having several options for selecting the best ED as well as the optimal antenna for offloading. Furthermore, the augmentation of UAV's transmit power enhances system offload performance since as the power grows up, so does the amplification factor, improving the signal forwarding.

Meanwhile, Fig. 4 illustrates the similar effect but with different numbers of antennae at BS. It is also remarkable that the analysis and simulation results ensure the consistency as well as offload performance can be improved by an increase number of antennae at both far and near BS, which can be explained by the best optimal antenna of UAV. Same as above, higher transmit power at the UAV contributes to better offload performance.

Fig. 5 expresses the effect of altitude of UAV (h_U) on SCPs with different numbers of ED. We see that there will be an optimal altitude that maximizes

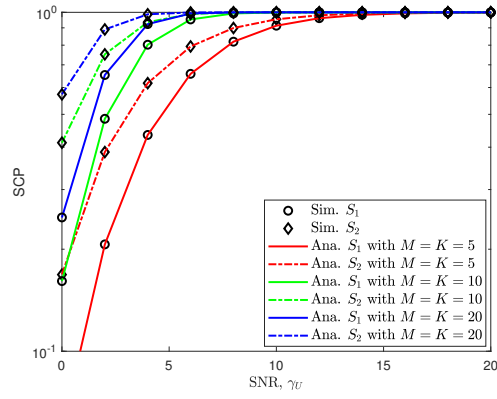


Fig. 4: Impact of average transmit SNR, (γ_U) on SCPs of the BS-MEC1 and BS-MEC2 with various M, K , $\gamma_0 = 1$, $(x_I, y_I) = (-100, -100)$, $(x_{B_1}, y_{B_1}, h_{B_1}) = (0, 200, 5)$, $(x_{B_2}, y_{B_2}, h_{B_2}) = (0, 150, 5)$, and $(x_U, y_U, h_U) = (0, 0, 150)$.

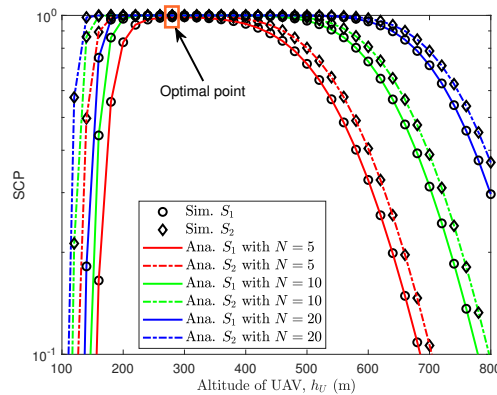


Fig. 5: Impact of altitude of UAV, (h_U) on SCPs of the BS-MEC1 and BS-MEC2 with various N , $M = K = 3$, $(x_I, y_I) = (-100, -100)$, $(x_{B_1}, y_{B_1}, h_{B_1}) = (0, 200, 5)$, $(x_{B_2}, y_{B_2}, h_{B_2}) = (0, 150, 5)$, and $(x_U, y_U) = (0, 0)$.

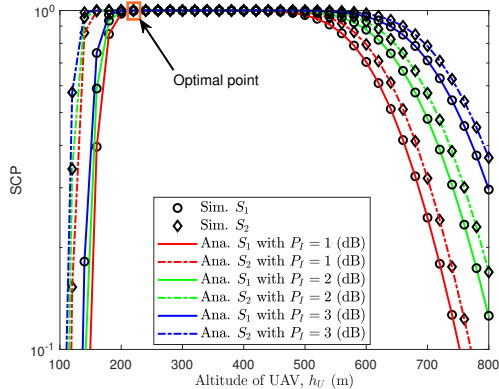


Fig. 6: Impact of altitude of UAV, (h_U) on SCPs of the BS-MEC1 and BS-MEC2 with various P_I , $M = K = 3$, $(x_I, y_I) = (-100, -100)$, $(x_{B_1}, y_{B_1}, h_{B_1}) = (0, 200, 5)$, $(x_{B_2}, y_{B_2}, h_{B_2}) = (0, 150, 5)$, and $(x_U, y_U) = (0, 0)$.

SCP. Because the altitude of the UAV affects the LoS and NLoS probabilities. When UAV operates at a low altitude, encountering NLoS is usual and LoS is uncommon. Moreover, obstacles in the urban environment will reduce communication between the UAV with the ED as well as the BS, thus leading to reduced offloading performance. As the altitude of the UAV increases, the probability of encountering LoS increases and NLoS decreases. Although the probability of NLoS between the UAV, ED and BS is reduced, the altitude of the UAV creates a very large gap between them, leading to severe transmission losses that also lead to reduced offloading performance. Therefore there will be an optimal altitude h_U^* to achieve maximum SCP.

Fig. 6 denotes this effect with different power transmit (P_I) of ED. The best suitable power for the maximum SCP is very important because transmission power of EDs has an impact on LoS and NLoS. Lower P_I leads to lower LoS and higher NLoS since the urban environment will reduce communication among the UAV, ED and BS, which can reduce offloading performance. By increasing the transmission power, LoS increases and NLoS decreases; however, consuming more power for transmitting promotes severe transmission losses, then reduces offloading performance. As a result, there will be an optimal transmission power to achieve maximum SCP.

In addition to the issue of UAV's altitude, we must also consider the location of UAV for better communication between it, ED, and the BS. Here is a 3D result depicting the value domain SCP resulting from the simultaneous effects of x_U and y_U . Fig. 7 shows the optimal position of the UAV according to BS-MEC1. We find that there exists a position x_U^* and y_U^* that optimizes system performance. This is understandable; UAV will choose the optimal location to communicate with ED as well as with the BS. This is considered a prominent feature of UAV.

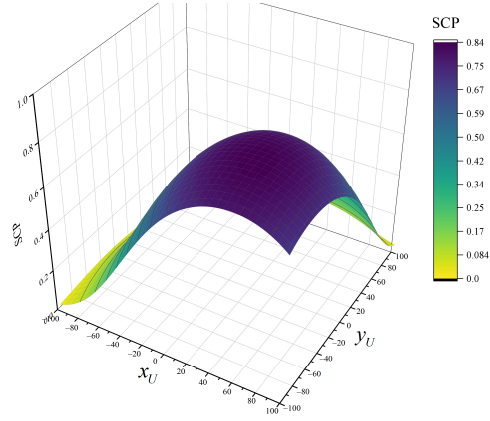


Fig. 7: Impact of location of UAV, (x_U, y_U) on SCP of the BS-MEC1 with $N = 20$, $M = K = 5$, $(x_I, y_I) = (-100, -100)$, $(x_{B_1}, y_{B_1}, h_{B_1}) = (0, 200, 5)$, $(x_{B_2}, y_{B_2}, h_{B_2}) = (0, 150, 5)$, and $h_U = 200$.

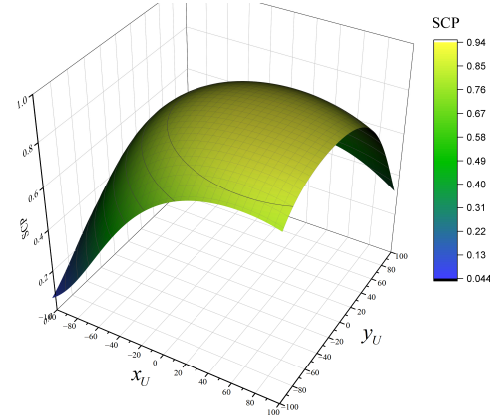


Fig. 8: Impact of location of UAV, (x_U, y_U) on SCP of the BS-MEC2 with $N = 20$, $M = K = 5$, $(x_I, y_I) = (-100, -100)$, $(x_{B_1}, y_{B_1}, h_{B_1}) = (0, 200, 5)$, $(x_{B_2}, y_{B_2}, h_{B_2}) = (0, 150, 5)$, and $h_U = 200$.

Table 1: Algorithm results.

N	S_1			S_2		
	x_{B_1}	y_{B_1}	h_{B_1}	x_{B_2}	y_{B_2}	h_{B_2}
5	23.6234	-58.7923	268.9456	-59.8878	0.2796	226.7227
10	34.2900	-55.2372	275.5536	-54.0102	14.9554	235.9151
15	41.3181	-52.8874	278.1054	-50.6816	23.1771	237.5701
20	45.2988	-51.5789	278.8993	-47.9684	26.0654	26.0654

On the other hand, Fig. 8 describes a 3D result about the optimal position of UAV the BS-MEC2. Calculation process proves the existence of optimal x_U^* and y_U^* for system performance. This is because of a striking feature of UAV: it will choose the optimal altitude for better communication with ED and BS.

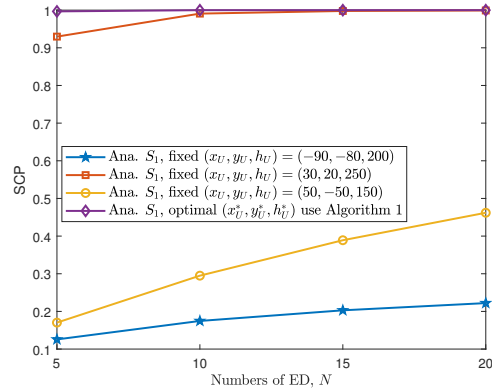


Fig. 9: Impact of location and altitude of UAV, (x_U^*, y_U^*, h_U^*) on SCP of the BS-MEC1 with $M = K = 5$, $(x_I, y_I) = (-100, -100)$, $(x_{B_1}, y_{B_1}, h_{B_1}) = (0, 200, 5)$, $(x_{B_2}, y_{B_2}, h_{B_2}) = (0, 150, 5)$.

Fig. 9 and Fig. 10 depict the impact of the position and elevation of UAV, (x_U^*, y_U^*, h_U^*) on the SCP of the entire system. We substitute the optimal values (shown in Table 1) found from solving the optimization problem proposed above (**Algorithm 1**). Specifically in Table 1, to find the optimal location for the UAV, if it prioritizes calculation and communication for BS-MEC1, the results will also be optimal for BS-MEC1, and the same thing happens when preferring BS-MEC2. The number of edge clusters of devices N has an influence on the SCP in certain cases, so different values of N are calculated and compared with each other to get the increasing relationship, because when N is larger, the values x_{B_1} , y_{B_1} and h_{B_1} are also larger. We compare $\text{SCP}(x_U^*, y_U^*, h_U^*)$ with SCPs with fixed (x_U, y_U, h_U) values, and the results show that applying the SCPMax-PSO

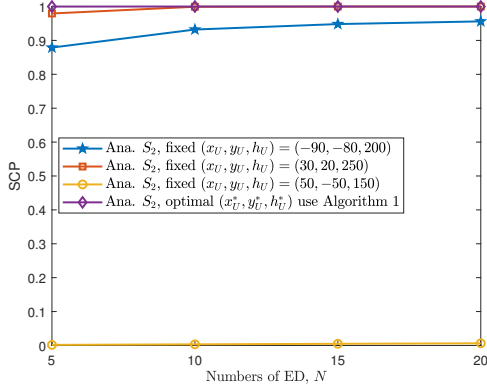


Fig. 10: Impact of location and altitude of UAV, (x_U^*, y_U^*, h_U^*) on SCP of the BS-MEC2 with $M = K = 5$, $(x_I, y_I) = (-100, -100)$, $(x_{B_1}, y_{B_1}, h_{B_1}) = (0, 200, 5)$, $(x_{B_2}, y_{B_2}, h_{B_2}) = (0, 150, 5)$.

algorithm to provide optimal values, the offload performance is best compared to if we manually set the UAV.

5 Conclusion

In this paper, we investigated the offloading performance of a UAV relay-assisted NOMA-MEC in IoT over Nakagami- m fading channel. We presented a four-phased protocol based on ED and antenna selection scheme, concentrated on NOMA-MEC techniques to increase the offloading performance. For system performance assessment, we obtain closed-form expressions of SCP of far BS-MEC and near BS-MEC. For SCP maximization, we introduced a PSO-based algorithm for determining the location and altitude of a UAV. We provided numerical results to validate the system's outsourcing performance. In addition, our future research will further explore the potential of maximal ratio combining and develop robust EH models for UWNMI systems.

A Proof of Lemma 1

(16) and (17) are substituted into (18), the S_1 of B_1 is rewritten as

$$\begin{aligned}
S_1 &= \Pr \left\{ X \geq \varphi_1, Y \geq \frac{\varphi_2 X + \varphi_3}{X - \varphi_1} \right\} = \int_{\varphi_1}^{\infty} \left[1 - F_Y \left(\frac{\varphi_2 x + \varphi_3}{x - \varphi_1} \right) \right] f_X(x) dx \\
&\stackrel{(S1)}{=} \theta_1 \sum_{j=1}^M \sum_{j_1=0}^j \sum_{i=0}^{N-1} \sum_{i_1=0}^i \theta_2 \theta_4 \int_{\varphi_1}^{\infty} x^{m+\bar{i}-1} \left(\frac{\varphi_2 X + \varphi_3}{X - \varphi_1} \right)^{\bar{j}} e^{-\frac{mj\varphi_2}{\Omega_1} \frac{\varphi_2 X + \varphi_3}{X - \varphi_1} - \frac{m(i+1)X}{\Omega_I}} dX \\
&\stackrel{(S2)}{=} \theta_1 \sum_{j=1}^M \sum_{j_1=0}^j \sum_{i=0}^{N-1} \sum_{i_1=0}^i \sum_{t_1=0}^{m+i-i_1-1} \sum_{t_2=0}^{\bar{j}} \theta_2 \theta_3 \theta_4 (\varphi_1)^{m+\bar{i}-1-t_1} \\
&\quad \times (\varphi_2)^{\bar{j}} (\varphi_4)^{\bar{j}-t_2} e^{-\frac{mj\varphi_2}{\Omega_1} - \frac{m(i+1)\varphi_1}{\Omega_I}} \int_0^{\infty} u^{t_1+t_2-\bar{j}} e^{-\frac{mj(\varphi_1\varphi_2+\varphi_3)}{\Omega_1 u} - \frac{m(i+1)u}{\Omega_I}} du \\
&\stackrel{(S3)}{=} 2\theta_1 \sum_{j=1}^M \sum_{j_1=0}^j \sum_{i=0}^{N-1} \sum_{i_1=0}^i \sum_{t_1=0}^{m+i-i_1-1} \sum_{t_2=0}^{\bar{j}} \theta_2 \theta_3 \theta_4 (\varphi_1)^{m+\bar{i}-1-t_1} \\
&\quad \times (\varphi_2)^{\bar{j}} (\varphi_4)^{\bar{j}-t_2} e^{-\frac{mj\varphi_2}{\Omega_1} - \frac{m(i+1)\varphi_1}{\Omega_I}} \left(\frac{j(\varphi_1\varphi_2 + \varphi_3)\Omega_I}{(i+1)\Omega_1} \right)^{\frac{t_1+t_2-\bar{j}+1}{2}} \\
&\quad \times K_{t_1+t_2-\bar{j}+1} \left(2m \sqrt{\frac{j(i+1)(\varphi_1\varphi_2 + \varphi_3)}{\Omega_1\Omega_I}} \right), \tag{22}
\end{aligned}$$

where $\theta_1 = -\frac{NM!(N-1)!}{(m-1)!} \left(\frac{m}{\Omega_I} \right)^m$, $\theta_2 = \frac{(-1)^j}{(M-j)!j_1!(j-j_1)!} \frac{(-1)^i}{(N-1-i)!i_1!(i-i_1)!}$, $\theta_3 = \frac{(m+i-i_1-1)!}{t_1!(m+i-i_1-1-t_1)!} \frac{(j-j_1)!}{t_2!(j-j_1-t_2)!}$, $\theta_4 = \left[\frac{1}{(m-1)!} \left(\frac{m}{\Omega_1} \right)^{m-1} \right]^{j-j_1} \left[\frac{1}{(m-1)!} \left(\frac{m}{\Omega_I} \right)^{m-1} \right]^{i-i_1}$, $\varphi_1 = \frac{\phi_1 L_{I*} U_R}{\gamma_0 [\rho - (1-\rho)\phi_1]} \frac{c_1^{off}}{c_1^{on}}$, $\varphi_2 = \frac{\phi_1 L_{U_R B_{1,*}}}{\gamma_1 [\rho - (1-\rho)\phi_1]}$, $\varphi_3 = \frac{\phi_1 L_{I*} U_R L_{U_R B_{1,*}}}{\gamma_0 \gamma_1 [\rho - (1-\rho)\phi_1]}$, $\varphi_4 = \frac{\varphi_2 \varphi_1 + \varphi_3}{\varphi_2}$, $\phi_1 = 2^{\frac{WT_1^{th}}{C_1}} - 1$. Step (S1), is obtained by substituting the PDF in (5) and CDF in (6). Step (S2) is obtained by changing the bound of the integral to $u = x - \varphi_1$. After a few mathematical transformations and applying the Bessel functions [15] we get the expression in Step (S3). This concludes our proof.

References

1. B. Li, W. Wu, W. Zhao, and H. Zhang, “Security enhancement with a hybrid cooperative NOMA scheme for MEC system,” IEEE Trans. Veh. Technol., vol. 70, no. 3, pp. 2635–2648, Mar. 2021.
2. A.-N. Nguyen, D.-B. Ha, V. N. Vo, V.-T. Truong, D.-T. Do, and C. So-In, “Performance analysis and optimization for IoT mobile edge computing networks with RF energy harvesting and UAV relaying,” IEEE Access, vol. 10, pp. 21 526–21 540, Feb. 2022.

3. A.-N. Nguyen, V. N. Vo, C. So-In, and D.-B. Ha, "System performance analysis for an energy harvesting iot system using a DF/AF UAV-enabled relay with downlink NOMA under nakagami-m fading," *Sensors*, vol. 21, no. 1, Jan. 2021.
4. Y. Xu, T. Zhang, J. Loo, D. Yang, and L. Xiao, "Completion time minimization for UAV-assisted mobile-edge computing systems," *IEEE Trans. Veh. Technol.*, vol. 70, no. 11, pp. 12 253–12 259, Nov. 2021.
5. Z. Ding, P. Fan, and H. V. Poor, "Impact of non-orthogonal multiple access on the offloading of mobile edge computing," *IEEE Trans. Commun.*, vol. 67, no. 1, pp. 375–390, Jan. 2019.
6. V.-T. Truong, V. N. Vo, D.-B. Ha, and C. So-In, "On the system performance of mobile edge computing in an uplink NOMA WSN with a multiantenna access point over Nakagami-m fading," *IEEE/CAA J. Autom. Sinica*, vol. 9, no. 4, pp. 668–685, Apr. 2022.
7. Y. Guo, C. You, C. Yin, and R. Zhang, "UAV trajectory and communication code-sign: Flexible path discretization and path compression," *IEEE J. Sel. Areas Commun.*, vol. 39, no. 11, pp. 3506–3523, Nov. 2021.
8. D. Liu, Y. Xu, J. Wang, J. Chen, K. Yao, Q. Wu, and A. Anpalagan, "Opportunistic UAV utilization in wireless networks: Motivations, applications, and challenges," *IEEE Commun. Mag.*, vol. 58, no. 5, pp. 62–68, May 2020.
9. H. Peng and X. Shen, "Multi-agent reinforcement learning based resource management in MEC and UAV-assisted vehicular networks," *IEEE J. Sel. Areas Commun.*, vol. 39, no. 1, pp. 131–141, Jan. 2021.
10. A.-N. Nguyen, V. N. Vo, C. So-In, D.-B. Ha, and V.-T. Truong, "Performance analysis in UAV-enabled relay with NOMA under Nakagami-m fading considering adaptive power splitting," in *Proc. Int. Joint Conf. Comput Sci. Software Eng.*, Jul. 2021, pp. 1–6.
11. A.-N. Nguyen, D.-B. Ha, V.-T. Truong, C. So-In, P. Aimtongkham, C. Sakunrasrisuay, and C. Punriboon, "On secrecy analysis of uav-enabled relaying noma systems with rf energy harvesting," in *Proc. Industrial Networks and Intelligent Systems*, Jun. 2022, pp. 267–281.
12. A.-N. Nguyen, V. Nhan Vo, C. So-In, D.-B. Ha, S. Sanguanpong, and Z. A. Baig, "On secure wireless sensor networks with cooperative energy harvesting relaying," *IEEE Access*, vol. 7, pp. 139 212–139 225, Sep. 2019.
13. A. -N. Nguyen, D. -B. Ha, V. N. Vo, V. -T. Truong, D. -T. Do and C. So-In, "Performance Analysis and Optimization for IoT Mobile Edge Computing Networks With RF Energy Harvesting and UAV Relaying," in *IEEE Access*, vol. 10, pp. 21526–21540, 2022.
14. J. Men, J. Ge and C. Zhang, "Performance Analysis for Downlink Relaying Aided Non-Orthogonal Multiple Access Networks With Imperfect CSI Over Nakagami-m Fading," in *IEEE Access*, vol. 5, pp. 998–1004, 2017,
15. I. Gradshteyn and I. Ryzhik, *Table of Integrals, Series, and Products*, A. Jeffrey and D. Zwillinger, Eds. USA: Academic Press, 2014.